Case Studies in Construction Materials 20 (2024) e03250

Contents lists available at ScienceDirect

Case Studies in Construction Materials

journal homepage: www.elsevier.com/locate/cscm

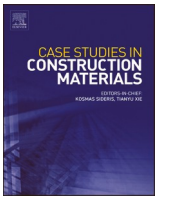

# Porous asphalt mixture performance in cold regions: Case study of Chicago

Renan Santos Maia [a], Yujia Lu [a], Ramez Hajj [b,*]

[a] Graduate Research Assistant, Urbana, IL 61801, USA
[b] Assistant Professor, Urbana, IL 61801, USA

ARTICLE INFO

*Keywords:*
Porous asphalt mixtures
Surface analysis
Binder aging
Gradation
CT scan
Internal structure
Dynamic modulus
Saturation degree

ABSTRACT

Porous Asphalt Mixtures (PAMs) improve resilience of flexible pavements in the context of climate change. PAM application in coastal cities like Chicago is of interest; however severe winters compromise the durability of PAMs given their susceptibility to freeze-thaw. This work aimed to evaluate the to-date experience with PAMs in Chicago, exploring benefits and limitations to be considered for future projects in the Southern Lake Michigan region. Full-depth PAM cores were obtained from seven sections, constructed in different years. Tests were conducted to assess the evolution of surface texture, internal structure, and multi-scale material properties. Regarding surface texture, consistent change over time was observed, such as loss of the "channel" structure, and increase in mean profile parameters because of raveling. Also, binder content varies with time within different layer depths. An aging gradient in terms of stiffness from top to bottom within the layer does not necessarily occur. However, binder ductility shows drastic and consistent reduction throughout the layer as aging increases. Analysis of internal structure using a CT scan revealed that there is also a lack of homogeneity in the air void and particle size distributions. Finally, this study suggests that full-depth PAM viscoelastic behavior is sensitive to saturation level, and this is a relevant subject to be considered, since partial saturation may be a condition often observed in the field.

## 1. Introduction

Efforts to increase infrastructure resilience have become a research topic of utmost importance, given the expected (and already observed) increase in frequency of extreme weather events, such as excessive rainfall, due to climate change. Resilience can be increased as the decision to invest in green infrastructure is made [1]. Qiao et al. [2] comprehensively reviewed the environmental stressors derived from climate change. Increase in temperature is the most commonly studied of these stressors. Higher temperatures will contribute to the overall reduction in modulus of asphalt pavements, as well as to accelerated aging of asphalt binder, leading to earlier deterioration and compromising the pavement life-cycle. Also, climate change modifies the dynamics of rainfall and groundwater. Extreme rainfall is detrimental to pavement mechanical performance, especially at high groundwater levels. Finally, the instabilities in climate when it comes to freezing temperatures can lead to an increase in the number of freeze-thaw cycles that a pavement will be subjected to during its service life. This last trend is already subject of interest in regions with mild winters, such as the Netherlands [3].

* Corresponding author.
*E-mail address:* rhajj@illinois.edu (R. Hajj).

https://doi.org/10.1016/j.cscm.2024.e03250
Received 9 February 2024; Received in revised form 13 April 2024; Accepted 2 May 2024
Available online 6 May 2024

Among the consequences of extreme weather events, flooding is one of the potential challenges that pavements may be more frequently subjected to. Porous Asphalt Pavements (PAP) are an engineered alternative to increase pavement resilience in face of extreme events. The porous structure, which includes a Porous Asphalt Mixture (PAM) on top of the pavement structure, is capable of storing and/or draining water during the rainfall event, reducing pressure on the drainage system [4,5]. The application of PAP concepts has emerged as a notable catalyst in the development of the "sponge city" concept [6], which refers to cities where infrastructure mirrors the functionality of a sponge system, facilitating absorption, infiltration, purification, and subsequent release of water from precipitation. When it comes to the context of the southern Lake Michigan area and its adaptation to climate change, coastal pavement infrastructure management is a critical issue. Now, more than ever, extreme weather events and climate change are causing more frequent flooding of pavement surfaces, which existing drainage schemes may not sufficiently handle [7,8]. Furthermore, the accumulation of water on the pavement surface results in a potential safety hazard and increased likelihood of crashes due to vehicle hydroplaning and increased stopping distance [9,10].

Asphalt mixtures are the most common material for surfacing American roadways, accounting for more than 90 % of U.S. roads. In general, a dense-graded aggregate gradation and a high degree of compaction are used to ensure the asphalt mix has satisfactory mechanical performance and good resistance to moisture infiltration, which is mainly represented by controlling an air void (AV) content around 4 %. However, the impermeability of this surface layer requires adequate drainage for water which appears at the pavement surface via rainfall or other climatic events. When extreme coastal events occur, surface drainage may not be adequate and the pavement surface can flood. This is one reason why opting for the use of PAPs and PAMs (the latter having an AV content around 20 %), instead of typical dense-graded mixtures, is seen as a potential solution for attenuating flooding-related issues.

The application of PAPs and PAMs is commonly observed in two ways: (i) Full-depth PAP, where water is drained through the pavement structure within a network of air voids in the asphalt layer placed over a stone reservoir (also called "recharge course"), or (ii) overlay PAP, where a PAM is placed over a traditional pavement structure with dense-graded asphalt concrete [11]. Although overlay PAPs have become more common, full-depth PAP structures have not been widely used in the United States, especially in cold regions [12] such as the southern Lake Michigan area, because of several challenges, including frost depth and subgrade frost heave, compromised freeze-thaw resistance of porous materials, limitations for cold weather construction, necessity of winter maintenance to control snow and ice, and accelerated deterioration of pavement performance due to winter maintenance [11]. Additionally, the general application of PAPs does not include high traffic sections, as it is typically limited to highway shoulders, parking lots, and local roads [11,13].

One of the main mechanisms for the development of distresses within asphalt mixtures is the aging of asphalt binder, comprising the composite structure of the asphalt concrete. Aging can be understood as detrimental molecular-scale changes of the asphalt binder,


**Fig. 1.** Locations of selected PAM cores in Chicago, IL.

largely derived from an oxidation process. Higher temperatures and higher availability of oxygen accelerate the aging process. Therefore, more severe aging is expected to happen at the surface of the asphalt layer, given the contact with atmospheric air, as well as with higher pavement temperatures. This trend is confirmed in many studies, for both conventional dense-graded asphalt concrete [14], as well as for overlay PAMs placed over dense-graded asphalt concrete [15]. When it comes to full-depth PAP, there is a lack of studies in this regard. It is well-known that, in the case of dense-graded mixtures, the aging level at the surface is significantly higher compared to the bottom of the full-depth asphalt layer. This trend has been documented in existing literature [14] for the state of Illinois, where dense-graded asphalt mixtures in full-depth pavements were divided into slices from different layer depths. The extracted binders from the bottom of the asphalt layer exhibited stiffness characteristics similar to laboratory-aged binders subjected to the Rolling Thin Film Oven (RTFO) aging protocol, representing short-term aging that occurs during the stages of mixing, hauling, and compaction. For dense-graded mixtures, after compaction, the air penetration depth is low, reducing the environmental aging effects at the bottom of the structure. This also explains the mechanism that makes extracted binders from the top-most surface of the asphalt layer the stiffest, similar to laboratory-aged binders subjected to more severe protocols, such as multiple Pressure Aging Vessel (PAV) aging cycles. Given that PAM is more permeable to both water and air, it is hypothesized that aging has the potential to penetrate deeper into the asphalt layer. Given the challenges that limit the use of PAMs in environments like the Southern Lake Michigan region, the objective of this research was to evaluate the to-date experience with PAMs in selected sections from Chicago, exploring what can be expected for future projects in the region, and providing insights for potential, suitability, and limitations of using this type of mixture. In order to accomplish this objectives, tests were conducted in the laboratory on field cores to assess the evolution of surface texture, internal structure, and multi-scale properties of materials, including the binder, aggregate, and mixture, over time.

## 2. Materials and methods

### 2.1. Acquisition of PAM field cores from Chicago, IL

Based on a preliminary literature review, better understanding the mechanisms that led PAM to be problematic in the southern Lake Michigan area was identified as the first step to approach the PAP application challenges. The research team connected with engineers working at the Chicago Department of Transportation (CDOT) to discuss their experience with PAMs. The general experience in Chicago was that porous asphalt use was not successful due to a variety of factors, such as the freezing susceptibility and the need for regular maintenance. However, Chicago has a considerable number of sections built over the last 15 years.

Based on the 15-year window of PAM use in Chicago, the research team worked with CDOT to obtain cores from seven porous asphalt sections located around the city. Fig. 1 shows the locations where the cores were sampled. In order to cover different distances from the shoreline, four of the selected projects can be considered to be close to the shoreline, while three of them are located in areas more distant from the shoreline. Data provided by CDOT for the mixes constructed after 2014 included mix design information for these materials, such as Asphalt Content (AC) (%), theoretical maximum specific gravity ($G_{mm}$), bulk specific gravity ($G_{mb}$), air void Content (AV) (%), voids in mineral aggregate (VMA), dust to asphalt binder ratio (D/A Ratio), gradation, and density. Part of this information is shown in Table 1. It was possible to say that the selected mixtures were considerably similar in terms of design (such as binder content between 5.6 % and 5.9 %, and air voids between 19.2 % and 20.5 %). All design gradations met the ASTM D-7064 (2021) standard limits (Fig. 2). Detailed construction data for sections 3 (year of construction = 2008) and 6 (year of construction = 2012) was not available. From the analysis of the asphalt binders extracted from the sections using Fourier Transformed Infrared (FTIR) Spectroscopy, it was possible to detect the presence of polymer-modification within the binders. The FTIR spectra indicated the presence of butadiene (one of the main components of styrene-butadiene-styrene polymer modifier (SBS)) at 966 $cm^{-1}$. SBS is commonly used in porous asphalt to improve the mixture durability [16]. Also, the analysis of the aggregates after extraction of asphalt binder shows the use of fibers during construction, which is a common practice for preventing the drain-down of the asphalt mixture during compaction.

Examination of Cook County soil property reports revealed that 96.7 % of the area exhibits moderate to high levels of frost action. Urban lands, however, have unique dynamics. As per the United States Department of Agriculture (USDA), potential for frost action refers to the probability of soil expansion either upwards or laterally due to the formation of segregated ice lenses (commonly known as frost heave), followed by subsequent soil collapse and loss of strength upon thawing. Frost action occurs as moisture migrates into the freezing zone of the soil. In the specific context of Urban Lands within Cook County, where the specimens under consideration were sourced, there are typically 170 frost-free days. Given that the exact number of freeze-thaw (FT) cycles is not available from a pavement management perspective, the “number of winter seasons” from the construction time until 2022 is a better parameter to differentiate sections. Other than that, estimates of the number of FT cycles based on fundamental studies from the University of

**Table 1**
Mix design information provided by CDOT.

| Section | Year of Construction | AC (%) | Gmm | Gmb | AV (%) | Field VMA | D/AC Ratio |
|---|---|---|---|---|---|---|---|
| 1 | 2020 | 5.7 | 2.501 | 1.990 | 20.5 | 29.0 | 0.61 |
| 2 | 2017 | 5.6 | 2.507 | 2.025 | 19.2 | 27.6 | 0.69 |
| 4 | 2017 | 5.7 | 2.517 | 2.020 | 19.8 | 27.8 | 0.75 |
| 5 | 2020 | 5.9 | 2.508 | 1.998 | 20.4 | 28.9 | 0.55 |
| 7 | 2014 | 5.8 | 2.504 | 1.998 | 20.2 | 30.0 | 0.50 |

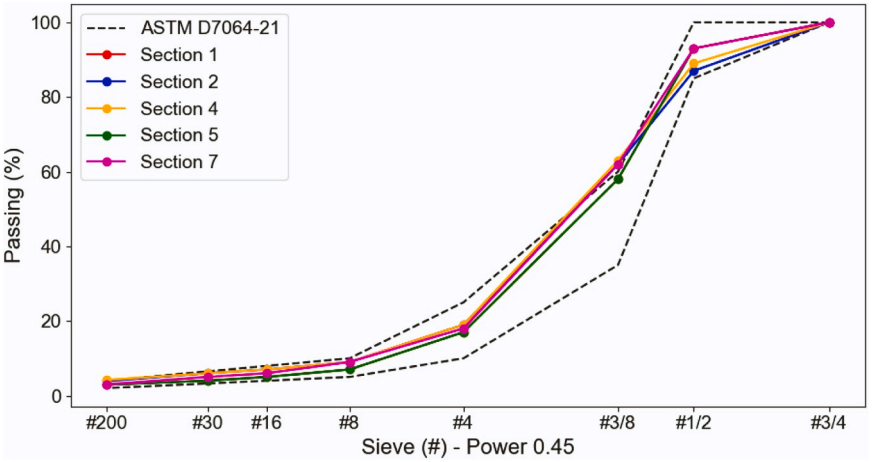


**Fig. 2.** Design gradations.

Illinois [17] can be made. This previous study encompasses extensive analyses on FT dynamics for studies on stabilized soils in Illinois. From the data gathered over the years, it is expected an approximate number of 10 FT cycles occur over 2 years, for the Northern Illinois area, which includes Chicago. This number varies from winter to winter and depends on the pavement structure. Fig. 3 summarizes the laboratory analysis performed.

### 2.2. Surface texture analysis

Surface texture is one of the critical elements of pavement performance affecting the ability of vehicles to safely stop over a specific distance during braking. It was assumed that all sections had similar initial texture, given the similarity of design parameters. Texture measurements are commonly conducted in the field, covering wider areas of the pavement. Alternative laboratory techniques may be applied when dealing with extracted cores. One of the recent advances in surface texture characterization is three-dimensional (3D) computer vision, by means of Close-Range Photogrammetry (CRP) [18,19]. In this research, CRP was applied to evaluate the pavement surface texture characteristics of the PAM sections. For this task, a smartphone camera was used to capture the images in

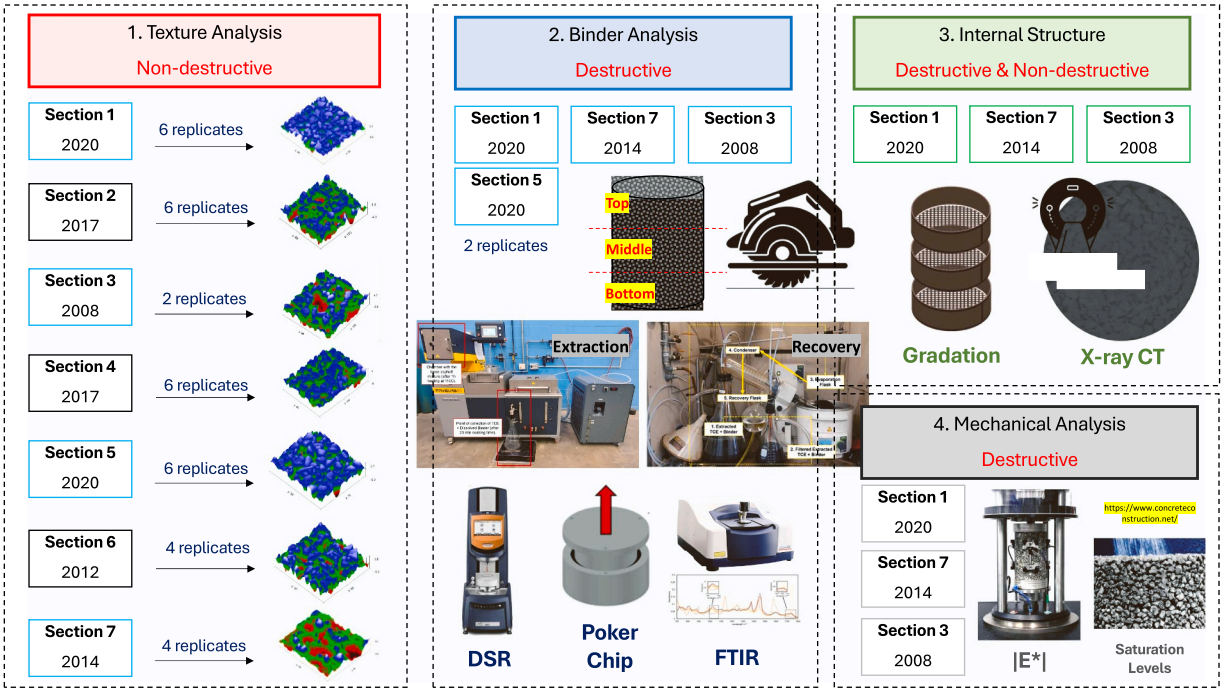


**Fig. 3.** Experimental framework.

counterclockwise direction from different spots of each core. At least 30 photos were taken per core, although a lower number (20 photos) would be enough. In each case, shaky and shadowed images were discarded, and homogeneous lighting quality and a reference scale were assured, as part of the method reported in recent literature [18,19]. Several computational tools can be used to quickly generate and analyze surface topographic meshes. In this research, the 3D meshes were built using Autodesk *Recap* software, and sub-sequentially exported as. *xyz* files for post-processing with *MeshLab* and *Gwyddion* computational tools. Basic area-based surface texture parameters were analyzed from each specimen. The meanings of the analyzed parameters are explained as follows:

- Arithmetical Mean Height (Sa): area-based surface parameter extended from the arithmetical mean height of a line (Ra). This provides an idea regarding the difference in height of each point in relation to the arithmetic mean of the surface.
- Root Mean Square Height (Sq): area-based surface parameter extended from the root mean square value of the sum of the squared difference between the profile points and the mean line (Rq).
- Skewness (Ssk): represents the degree of bias of the roughness shape (asperity).
- Kurtosis (Sku): represents the sharpness of the roughness profile.
- Density of Peaks (Spd): represents the number of peaks (per unit area).
- Peak Material Volume (Vmp): represents the volume of material at the threshold of 10 % of material ratio.

### 2.3. Asphalt binder analysis

Four PAP sections were selected for this phase. The selected sections covered different years of construction (2008, 2014, 2020), with a 6-year gap between each other. For construction year 2020, two sections were selected in order to evaluate potential surrounding environment characteristics that can lead to different performance according to the location of the section in the city. This includes being close/far to the lake-shore, being more/less wide or being subjected to lower/higher levels of sunlight (as a function of presence of shadow from trees and buildings in the surroundings).

The selected field cores were sliced in layers of 50 mm each by using a block saw. Limitations for defining the layer thickness for this work included producing slices at least three times thicker than the mixture Nominal Maximum Aggregate Size (NMAS) of 12.5 mm, and sufficiently thick so the amount of recovered binder would be sufficient for conducting Frequency Sweep (FS) with the Dynamic Shear Rheometer (DSR), Poker Chip (PC), and Fourier-transform Infrared Spectroscopy (FTIR) tests. The extraction of asphalt binder from each 50 mm slice was performed using an auto-extractor. The extraction and recovery protocol conducted in this research followed steps defined in previous literature [14]. The auto-extractor used trichlorethylene (TCE) as the contact medium for the pre-heated asphalt mixture (30 min at 140°C). During a soaking period of 20 min, the binder was dissolved in TCE. The resulting solution, comprised of TCE and dissolved binder, was collected in a beaker and subsequently transferred to the recovery station. In the recovery station, the solution underwent filtration to remove any remaining fine particles. The TCE was then separated from the binder through a distillation process involving boiling and condensation by means of the rotary evaporator (ASTM D5404/D5404M-21, AASHTO T319–22) equipment.

The combination of binder tests conducted in this research allows for a more comprehensive analysis of the “aging penetration”

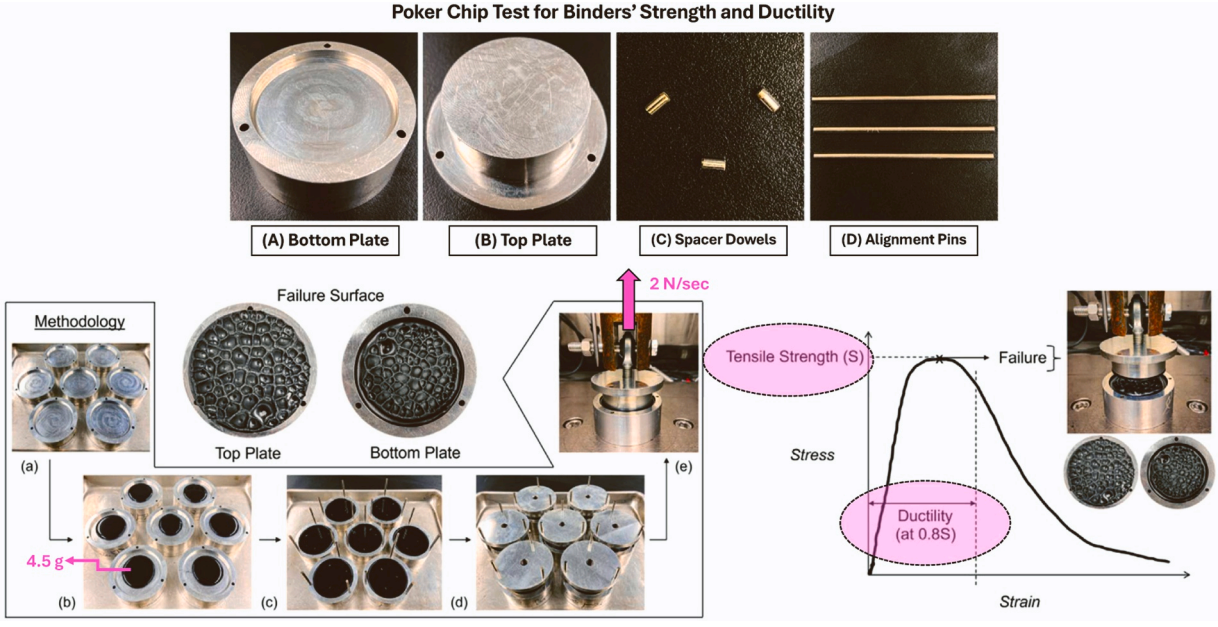


**Fig. 4.** Poker Chip testing protocol (adapted from Vyas et al. [23]).

within the PAM layer, namely: Frequency Sweep (FS), Poker Chip (PC), and Fourier Transformed Infrared (FTIR) Spectroscopy were used. The FS test was conducted to measure the linear viscoelastic (LVE) properties of the binder. The FS tests were conducted in accordance with AASHTO T315–06 at temperatures of 15, 25, 35, and 45°C, covering frequencies ranging from 0.1 to 10 Hz to construct master curves. The sigmoidal function and Williams-Landel-Ferry (WLF) [20] shift factors were determined to facilitate time-temperature superposition for fitting test data and obtaining master curves at 25°C. The obtained results were compared to a database of 7 different binders. These binders cover all the main Performance Grade (PG) labels used in the state of Illinois for roadway applications. The mentioned database had binders evaluated at different aging levels (unaged, RTFO-aged, and PAV-aged). For comparison, the master curves of the recovered binders were plotted together with the PAV-aged database of binders. In addition to evaluating the linear viscoelastic properties, the extracted binder was also assessed in the non-linear region. The Poker Chip (PC) test was employed to measure the intermediate temperature anti-cracking resistance of the binder, allowing for a comparison of properties at different depths. In this test, tensile loading of 2 N/sec was applied to a confined thin film of binder until cohesive failure occurred (Fig. 4). The determination of the loading rate was based on the findings of previous researchers [21]. The strength (peak stress) and ductility (accumulated strain until a 20 % drop of the peak stress) of the binder were derived from the results of this test. For a more detailed description of the test geometry [22], procedure, and data interpretation, refer to the works by Filonzi et al. [21] and Vyas et al. [23].

Finally, FTIR spectra were obtained for the extracted binders from 400 to 4000 $cm^{-1}$ at a resolution of 0.4 $cm^{-1}$ using attenuated total reflection (ATR) mode. Three replicates were analyzed from each binder (two from each section: top and bottom). Each sample was scanned 50 times to average the results. Absorbance spectra were analyzed using integration-based computation by calculating the area under the FTIR spectrum between the bands of interest [24,25]. The Carbonyl index (CI) and Sulphoxide indicex (SI), which are often used as aging indicators [26,27], were computed by Eqs. (1) and (2), respectively.

$$CI = A_{1700}/(\sum A_{1325-1515} + \sum A_{1535-1650}) \tag{1}$$

$$SI = A_{1030}/(\sum A_{1325-1515} + \sum A_{1535-1650}) \tag{2}$$

where $A_{1030}$ and $A_{1700}$ represent the absorption peak area at the wavelength around 1030 $cm^{-1}$ and 1700 $cm^{-1}$. The CI and SI index were normalized by the aliphatics and aromatics peak areas. $\sum A_{1325-1515}$ is the area of the absorption peak of aliphatics while $\sum A_{1535-1650}$ is the area of absorption peak of aromatics.

### 2.4. Aggregate gradation analysis

After obtaining TCE + binder solution from auto-extraction for recovery, the mix remaining inside the machine was subjected to additional 10 cycles of washing and 5 cycles of drying. Afterwards, the aggregates were subjected to sieve analysis. In this phase, changes in gradation of the PAM related to layer depth were evaluated.

### 2.5. Internal structure analysis

X-ray computed tomography (CT) analysis provides an idea about the internal structure of materials by passing x-rays through their structure and measuring the amount of x-ray detected on the other side. By repeating this at many different angles, the machine can read the linear density profile in many directions and therefore convert the detected x-rays to density distributions, creating 2D "slices" of the material, and revealing its micro-structure based on components having different densities. Although the field as-built data records one single value for AV, it is known that this AV content is heterogeneously distributed through the asphalt layer. Previous studies analyzed AV distribution using CT scans for dense-graded mixtures [28–31], and PAMs [32–34]. In this study, an x-ray CT acquisition system at the Institute for Genomic Biology (IGB) at the University of Illinois was used. The x-ray source had 225 kV voltage, 1000 $\mu$A current, and 225-micron focal spot size. The effective distance between slices was 100 microns.

Radial PAM slices obtained by x-ray CT were employed to develop 2D aggregate gradations and 2D AV distributions. To verify the gradation obtained using the non-destructive technique, 3D gradation of each PAM sample was converted to 2D gradation by inverse stereology and is considered as a reference. In this section, three cores (Sections 1, 3, and 7) from different years were analyzed to understand the effect of service life. In each core, at least two layers were analyzed to represent samples from distinct thicknesses.

Inverse stereology is a process of obtaining the 2D gradation based on a 3D grain distribution function. Filonzi et al. [35] showed that the polyhedral assumption for aggregate particles was realistic because the aggregates are angular particles with different shapes. The inverting calculation procedure was developed by Wicksell [36] for spherical particles and revised for polyhedral samples by Zhang [37] as shown in Equation (3) [35].

$$\phi(r) = \int_r^{R_{max}} \left(\frac{P_{max} - P_{min}}{R_{max} - R_{min}}\right) \frac{1}{x} \mathrm{d}x \tag{3}$$

where: $\phi(r)$ is the 2D gradation percentage passing size $r$; $R_{max}$ and $R_{min}$ are the maximum and minimum particle sizes in consecutive sieves; $P_{max}$ and $P_{min}$ are the percentage of particles with maximum and minimum particle sizes.

Images obtained from CT scans were analyzed using *FIJI* software [38]. The segregation method based on machine learning was used in this study because it shows a better performance in differentiating between air voids and asphalt mortar, compared to

traditional color threshold method, which is more arbitrary because of the uncertainty of energy intensity differences in each image, and operator skill [39]. Generally, the image processing approach can be broken into four steps as shown in Fig. 5:

1. Create an area of interest (AOI) mask based on to exclude the background and boundary areas from the asphalt mixture.
2. Segment the aggregate and voids based on Trainable Weka Segmentation plug-in (Machine learning algorithm) to create a new image.
3. Select the aggregate portion of particles and apply watershed segmentation in the new image to obtain the aggregate's closest elliptical diameter distribution.
4. Select air voids for analyzed particles in the new image to obtain the air void area percentage.

### 2.6. Mechanical analysis

One of the objectives of this research was to assess the mechanical behavior of PAMs in different conditions, namely, with a different number of winter seasons experienced in the field, and at different saturation degrees. Given the limitations in terms of coring (the older the section, the more difficult it is to perform adequate saw-cutting of specimens with them remaining intact), dynamic modulus ($E^*$) tests were performed for sections 1 (2020), 5 (2020), and 4 (2017). The 2017 section was subjected to 3 winter seasons more than the first two sections. Furthermore, as shown by Rueda et al. [40], the saturation degree of the asphalt mixtures informs the viscoelastic properties of asphalt mixes, where filling air voids with water may increase modulus magnitude by the replacement of air with an incompressible fluid. Therefore, PAM cores initially tested were subjected to a simplified 2-hour conditioning time in a water bath (at 25°C) and re-evaluated in terms of $E^*$.

The dynamic modulus test was conducted as per AASHTO standards T342–11 (2019), T378–17 (2021), and R84–17 (2021). The AASHTO T378–17 (2021) standard was the main reference for performing the $E^*$ test by means of the Asphalt Mixture Performance Tester (AMPT) for determination of stiffness and phase angle. The test was conducted for each specimen at 4.0, 20.0, and 40.0°C, at three loading frequencies: 0.1, 1, and 10 Hz for the first two temperatures, and four frequencies: 0.01, 0.1, 1, and 10 Hz for the last temperature. A controlled sinusoidal compressive loading was applied to the cylindrical specimens, and peak-to-peak strains were fixed between 75 and 150 micro-strain to ensure that the mixes were within the linear viscoelastic (LVE) region and that no damage was introduced during testing. The master curves for each mix were built based on the time-temperature superposition principle. The sigmoidal function in Equation (4) was employed to fit the master curves at reference temperature of 20.0°C. The Williams-Landel-Ferry (WLF) Equation (Equation (5)) [20] was used to determine shift factors.

$$\log|E*| = \delta + \frac{\alpha}{1 + e^{\beta+\gamma(\log f_r)}} \tag{4}$$

where:

- $f_r$: reduced frequency.
- $\alpha$, $\beta$, $\gamma$: curve fitting coefficients.

$$\log a_T = \frac{C_1(T - T_0)}{C_2 + T - T_0} \tag{5}$$

where:

- $C_1$, $C_2$: fitting coefficients.
- $T_0$: reference temperature (20.0°C).
- $T$: temperature to be shifted.

The tested specimens were subjected to moisture conditioning and subsequently tested again at 20°C and a wider range of frequencies: 25, 10, 5, 1, 0.5, 0.1, and 0.01 Hz. The specimens were tested in a partial saturation condition as described above.

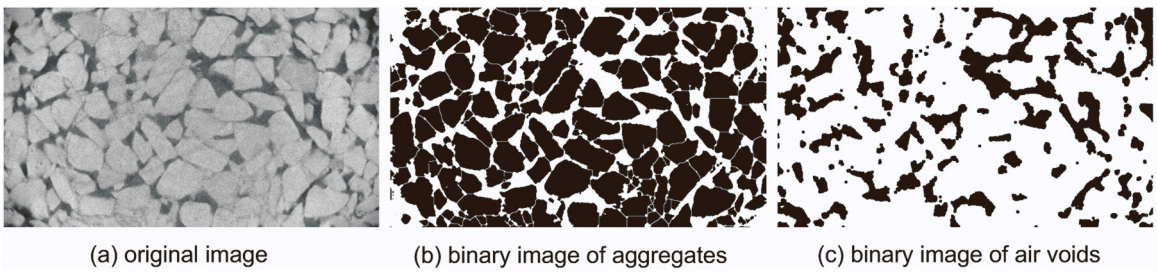


**Fig. 5.** Typical CT scanning image process.

## 3. Results and discussion

### 3.1. Surface texture analysis

The main goal of this analysis was to assess the evolution of surface texture parameters in the PAM cores with respect to time (from the oldest to the most recent PAM sections). Fair $R^2$ values [41] were obtained for the relationships between texture parameters and the age of sections. It should be reinforced that the evolution of texture parameters is influenced by other factors besides age only, but of course time in service has considerable effect. Other factors can affect this phenomenon: (i) construction quality, (ii) traffic level, (iii) local weather (given that the sections are located in different areas in Chicago, precipitation, snow, wind, and temperature levels can slightly vary), (iv) maintenance activities (such as snow accumulation and removal), and (v) pollution (the amount of particulate material can vary among the different sections). Finally, it should also be noted that specific details of materials, even considering the similarity in terms of mix design, change with time, so specific characteristics of materials at each section's construction time may represent additional variability. The trends in terms of surface texture are summarized in Fig. 6.

From the analysis of Fig. 6, Sa and Sq exhibited a relative increase with aging, indicating a progressive coarsening of the pavement surface ($R^2 = 0.57$ and 0.51, respectively). Furthermore, SSk, exhibited a less negative value with aging, representing a trend of a more symmetrical texture distribution ($R^2 = 0.61$), which is also an indication of the loss of the channel structure and potential clogging. Sku remained below 3 for all cases, but clearly increases with aging ($R^2 = 0.67$), indicating that the observed raveling and disintegration of coarse aggregates points to the increase of the sharpness of the texture profile. Observations from the field corresponded to these texture analyses, with Section 7 (constructed in 2014) showing increased raveling, while Section 3 exhibited a propensity for disintegration because of the damaged state of the PAM layer. This trend is also captured by the analysis of the peaks (Fig. 7). The material peak volume (Vmp) also increases with time, because of the loss of aggregates, which creates new peaks within the surface. The density of peaks (Spd) initially decreases in function of initial polishing of the surface, but as the loss of aggregates increases with time, new peaks are created, and Spd increases again. The initial polishing observed by Spd is not captured by the volumetric parameter (Vmp).

### 3.2. Asphalt binder analysis

#### 3.2.1. Binder content

In terms of binder content (%) differential between top and bottom layer surfaces (Table 2), the less-aged sections (1 and 5, from 2020) presented higher binder content within the bottom of the PAM layer. This is a result of a movement of finer particles from the top to the bottom of the layer, as a function of the freedom of movement within the void channels, during placement and compaction, confirmed with the analysis of the fine aggregate content (shown in the next section), for which both sections 1 and 5 had more fines in the bottom layer as well. Given that finer particles have higher surface area, a higher binder content was expected for the bottom of the PAM layer, as well as a slightly lower AV content. Furthermore, at early stages of the service life, there is no discernible effect of the washing of the binder film with water flow. Also, there is still no impact of the increased brittleness of the mixture that is expected to happen over time. Consequently, during the initial years, particles maintain cohesion and adhesion within the layer, minimizing the detachment of particles which ultimately also carries the binder film away at the top of the layer. Fig. 8 illustrates this.

As the PAM layer ages, there will be more wearing of the binder film at the surface, exposing the aggregates' texture and later polishing this texture. However, it was found for sections with more than 8 years in service that the binder content at the bottom of the

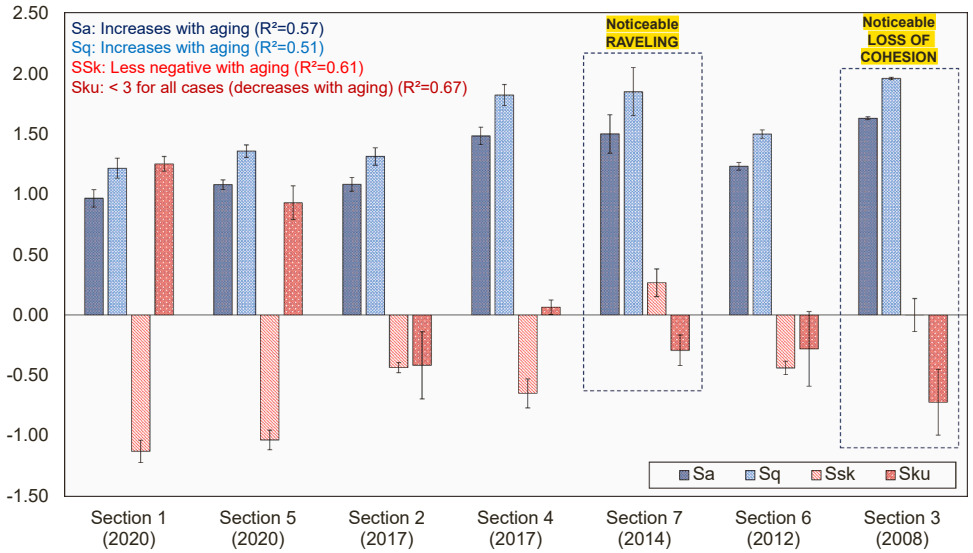


**Fig. 6.** Surface texture analysis.

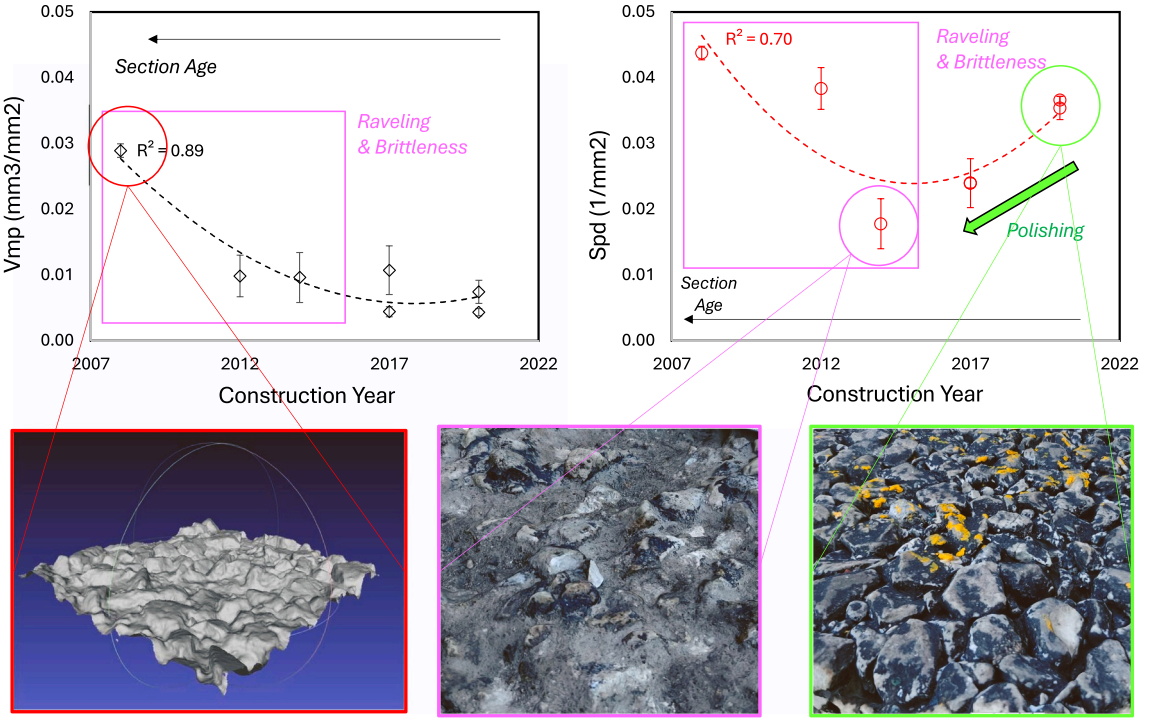


**Fig. 7.** Analysis of surface peaks.

**Table 2**
Binder content (%) variation between top (surface) and bottom.

| Section | Year | Top | Bottom | Variation (%) | Interpretation |
|---|---|---|---|---|---|
| 1 | 2020 | 4.6 | 5.3 | -0.7 | Fines' Movement and Surface Polishing |
| 5 | 2020 | 5.7 | 6.0 | -0.2 | Fines' Movement and Surface Polishing |
| 7 | 2014 | 5.5 | 4.9 | 0.6 | Washing and Disintegration |
| 3 | 2008 | 5.8 | 5.2 | 0.6 | Washing and Disintegration |

layer was even lower than the content at the surface. The explanation for this consists of two phenomena: (i) water flows through the PAM layer, detaching the binder film from the aggregates, and washing it away into the choker course; (ii) the increased brittleness of the PAM with time favors the detachment of particles, and this detachment is more pronounced at the bottom of the PAM layer, given that especially finer particles are also washed away. These trends are also illustrated in Fig. 8. Furthermore, in all cases, the asphalt binder extraction revealed a consistent pattern of lower binder content in the field cores compared to the design binder content, particularly in the surface layer. This does not necessarily imply a construction issue. Actually, the asphalt binder may be washed away quickly in these types of mixes due to moisture-induced detachment of the binder film at the binder-aggregate interface. For instance, texture analysis conducted on sections 3 and 7, which had been in service for 12 and 8 years respectively, exhibited an increased occurrence of surface raveling. Considering that the binder is the fundamental material responsible for ensuring the cohesiveness of the composite structure, the presence of lower binder contents raises concerns regarding the weakening of the binding forces that hold aggregates together.

### *3.2.2. Frequency sweep*

The binders recovered from the different thicknesses were analyzed using frequency sweep master curves as a surrogate for the level of aging experienced by the material. Fig. 9 shows the master curves of binder complex modulus for sections 1, 5, 7, and 3, respectively, and each curve was put in perspective to a database [23] of 7 binders of different PG grades typically used in the state of Illinois, aged up to the PAV level. For sections 1 and 5, the master curve was fitted completely below the PAV-level line obtained from the Illinois' typical asphalt binders' database, indicating that these sections did not reach the expected long-term binder aging level used as reference. Oxidation was expected to increase from the newest (1 and 5) to the oldest sections (7 and 3) for the top (surface) layer.

An uncertain trend was expected when it comes to the variation of aging relative to depth, given the lack of literature indications regarding this variation for full-depth PAMs. In sections 1 (2020, 2 years in service) and 7 (2014, 8 years in service), no significant

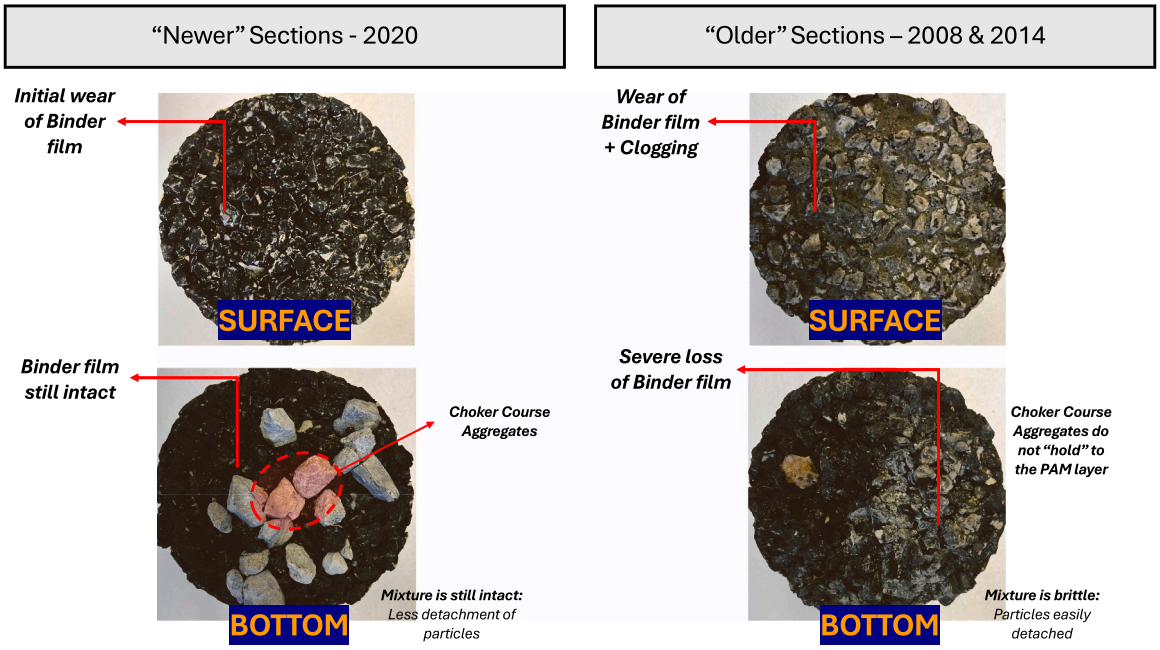


**Fig. 8.** Visual analysis of PAM sections' top and bottom surfaces.

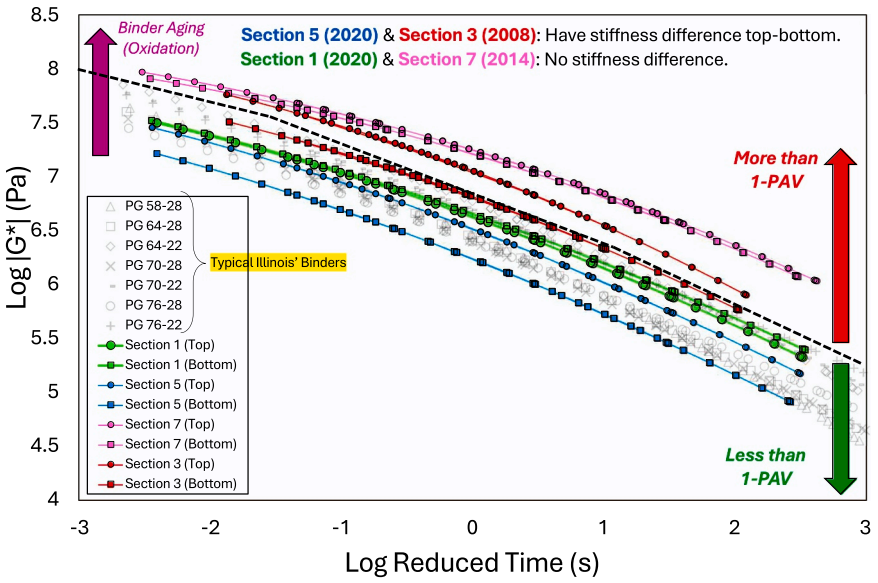


**Fig. 9.** PAM binders' master curves compared to typical binders used in Illinois (PAV-aged).

difference in the recovered binder was observed between the top and bottom of the PAM layer. However, in sections 5 (2020, 2 years in service) and 3 (2008, 14 years in service), a more noticeable difference was observed, with the binder being stiffer at the top of the layer. The first outcome from these results was an affirmation that "age" or "time in service" is not the only mechanism driving the aging gradient in relation to thickness. When comparing the two sections constructed in the same year (section 1 and section 5, both in the year 2020), the difference between the surface and bottom was only noticeable in section 5, where the surface binder exhibited higher stiffness compared to the bottom binder. Further investigation revealed that section 5 was wider than Section 1, and located in a more open space with less tree shadows. These factors contribute to increased exposure of the surface of section 5 to UV radiation, which may have played a role in the observed difference in binder stiffness between surface and bottom.

### 3.2.3. Poker chip testing

The results of the PC test are presented in Fig. 10. When comparing the two sections with the same age (Section 1 and Section 5), the strength at the top and bottom of Section 1 was similar. However, in Section 5, the strength at the bottom was lower, indicating that the surface of Section 5 experienced more aging related to increased stiffness, which confirms the trend observed with the stiffness of binder with frequency sweep, where, for Section 5, the stiffness of the recovered binder on the top of the surface was noticeably higher. In terms of ductility, Section 5 exhibited higher ductility at the bottom compared to the top, again indicating that the top of the layer had undergone more aging and become more brittle. The ductility of Section 1 binder was slightly higher at the bottom, suggesting a less clear aging gradient. For Sections 7 (constructed in 2014) and 3 (constructed in 2008), the ductility decreased significantly compared to Sections 1 and 5 (both constructed in 2020), indicating an increase in binder brittleness. The ductility values for both top and bottom of Sections 7 and 3 were similar, suggesting that aging and loss of ductility, resulting in increased brittleness, had penetrated throughout the full depth of the PAM layer.

### 3.2.4. FTIR

FTIR indices were computed to assess the oxidation level variation among each of the 4 evaluated sections in different layers (top/bottom), as shown in Fig. 11. Results showed that sections 5 (2020) and 3 (2008) presented a more significant drop in terms of CI from top to bottom, meaning a lower oxidation level. This finding corroborates that of the master curves, where sections 5 and 3 also presented a clear variation, being the top of the PAM stiffer in terms of G* than the bottom. It should be noted that the analysis of FTIR spectra is not ideal to compare different binders, such as the ones obtained from different locations in this study. The limits of FTIR were revealed in the study by Marsac et al. [24]. The common use of FTIR is for relative measurement of the same initial binder or mixtures at different stages, for example, a binder before and after aging, or before and after processes such as rejuvenation or polymer modification. For comparison between different binders, trends may be unclear and make it difficult to draw conclusions. No significant differences were observed in terms of CI for sections 1 (2020) and 7 (2014), which also corroborated results of the master curves shown in Fig. 9. However, for section 3, even with the observed gradient of oxidation from top to bottom (from FTIR CI and master curves), the ductility of the binder remained approximately constant, at a level below 0.3. Sections 3 and 7 presented similar SI for top and bottom, and, although a gradient was observed for CI for section 3, ductility of both binders from sections 3 and 7 remained approximately constant and in a lower level. The SI increase is expected when binders reach a PAV-level of aging [42]. However, at the level of aging of sections 3 and 7, ductility remains low and approximately constant even with eventual differences in terms of CI and SI indices.

## 3.3. Gradation analysis

The variation of gradation with layer depth (especially top/bottom) was assessed after binder extraction for the PAM specimens obtained from the years 2020, 2014, and 2008. For the 2020 sections (approximately 2 years in service in the field), gradation remained approximately stable through different layers (Fig. 12). Still, there is a slight trend of a finer gradation for the bottom-most layers, as shown for section 1, where the gradation curve moves upwards as the depth increases. This was seen as a compaction-related issue for PAMs. Once the loose PAM is placed and compacted in the field, finer particles tend to be displaced to the bottom of the layer, given that there is more freedom of movement of these particles downwards by gravity in function of the high volume and interconnection internally within the void network. For the sections with more than 8 years in service (Sections 3 and 7), the clogging effect becomes more observable, as shown in the gradation plots in Fig. 12. It can be seen that for both sections 3 and 7, the amount of

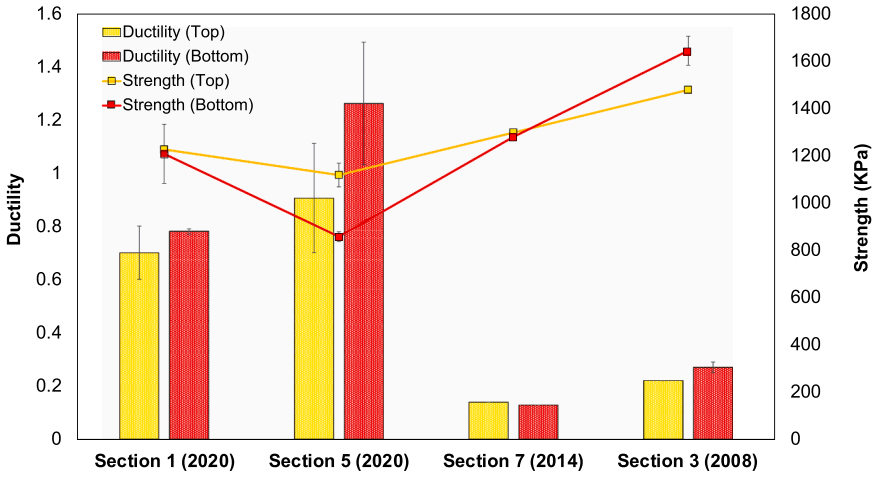


**Fig. 10.** Strength and ductility variation with layer depth.

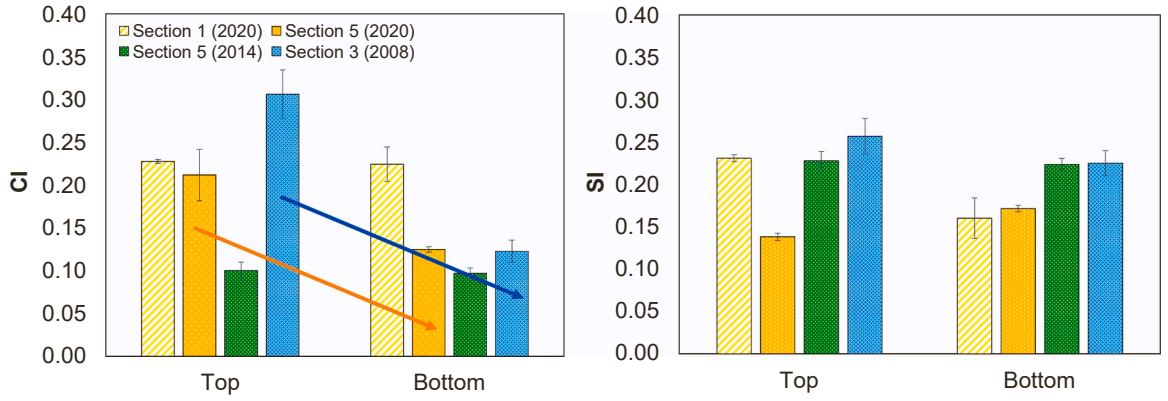


**Fig. 11.** FTIR CI and SI variation with layer depth.

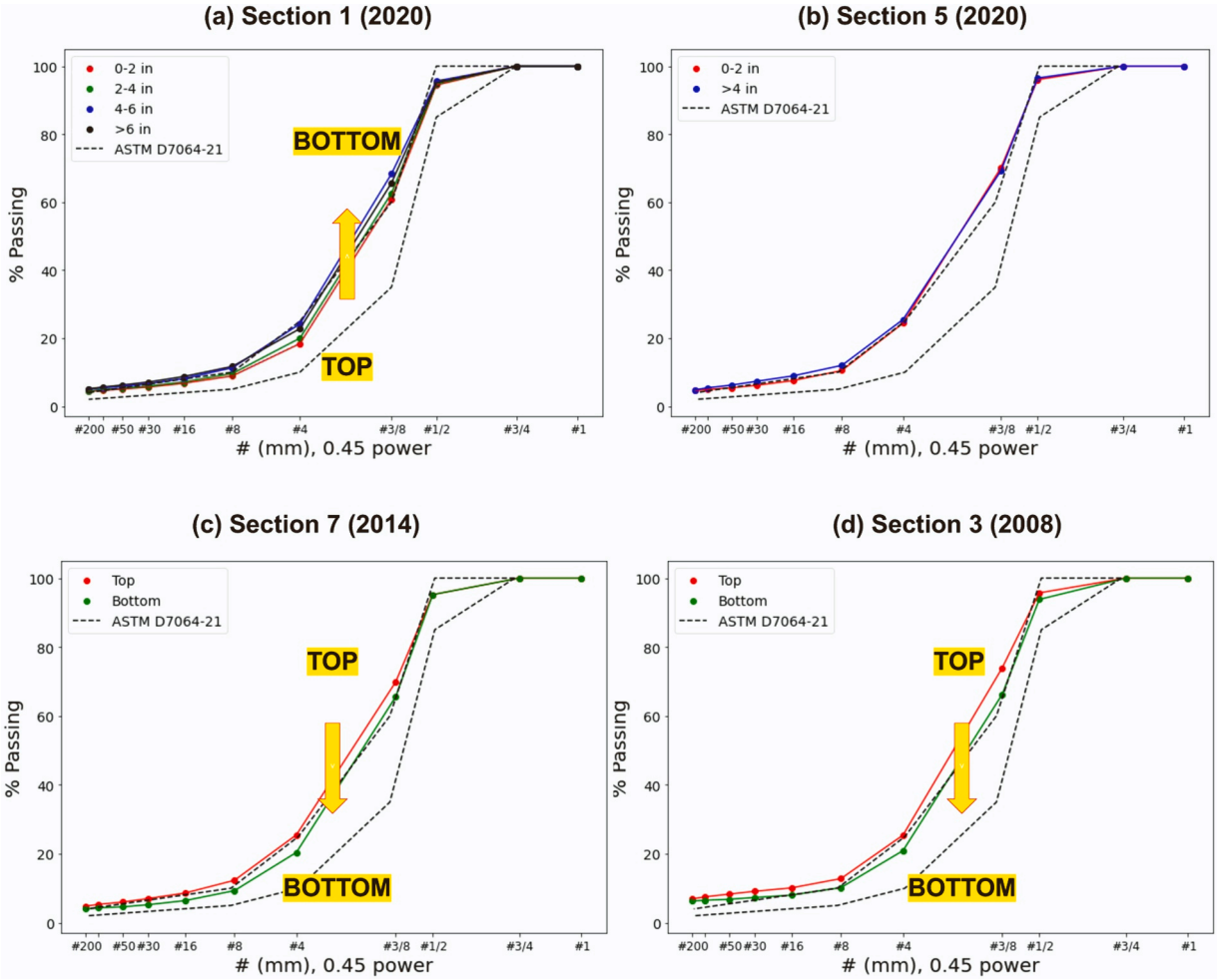


**Fig. 12.** Gradations' gradient with depth.

particles passing the #8 sieve is higher at the top of the layer. From the analysis of the four sections, 8 years in service showed to be a time whose differences in the amount of fines between top and bottom became more sound. Also, 14 years in service showed to be a time that even the bottom of the PAM layer starts to show an increased amount of fines, explained by the fact that the water that constantly flows inside the PAM will progressively carry fines deeper into the layer.

In terms of gradation, there is a clear trend that, in both sections 3 (14 years in service) and 7 (8 years in service), the amount of

material passing the #3/8 size is higher than the standard, and higher at the top compared to the bottom layer. This is probably an effect of the ravelling of the surface captured by the texture analysis of 3D models. This highlights the effects of moisture and freeze-thaw. The mechanisms of moisture damage and freeze-thaw start to develop when water infiltrates the PAM layer and gets trapped inside its structure. Once waters remains in the internal structure of the PAM, chemical and physical reactions can favor the detachment of the binder film from the aggregate surface, weakening the adhesion at the binder-aggregate interface. At the same time, water that gets trapped inside a non-connected void will expand at freezing temperatures, generating micro-cracks which eventually lead to distresses. Once the adhesive forces that bind aggregate and binder are weakened, ravelling tends to occur causing coarse aggregates to be exposed at the surface of the asphalt pavement and in turn more easily detached with traffic.

It is evident, therefore, that the surface of the PAM layer is subjected to a combination of factors, including clogging, moisture damage, and freeze-thaw. An additional explanation for the occurrence of raveling is the aging process and subsequent increased brittleness of the asphalt mixture. Furthermore, variations in binder content during construction can have detrimental consequences regarding susceptibility to raveling. When the PAM is constructed with a lower-than-designed binder content, the resulting binder film connecting the aggregate particles becomes thinner. This, in turn, renders it more susceptible to adverse effects of moisture and freeze-thaw, ultimately leading to distresses such as raveling.

### 3.4. Internal structure analysis

The 2D gradation curves obtained from a conversion based on actual sieve analysis (shown as converted 2D in Fig. 13) verified the efficiency of the internal structure analysis approach based on CT-scan. Fig. 13 also shows the CT scan figures of top and bottom layers for different sections and their 2D gradation results. Similar to gradation analysis from extracted PAM layers, sections 3 and 7 in Fig. 13 indicated more fines remained on the top layer due to clogging. It should be noted that a difference between gradation from CT scan slices and extracted aggregate distribution exists because the destructive and non-destructive tests employed samples from same

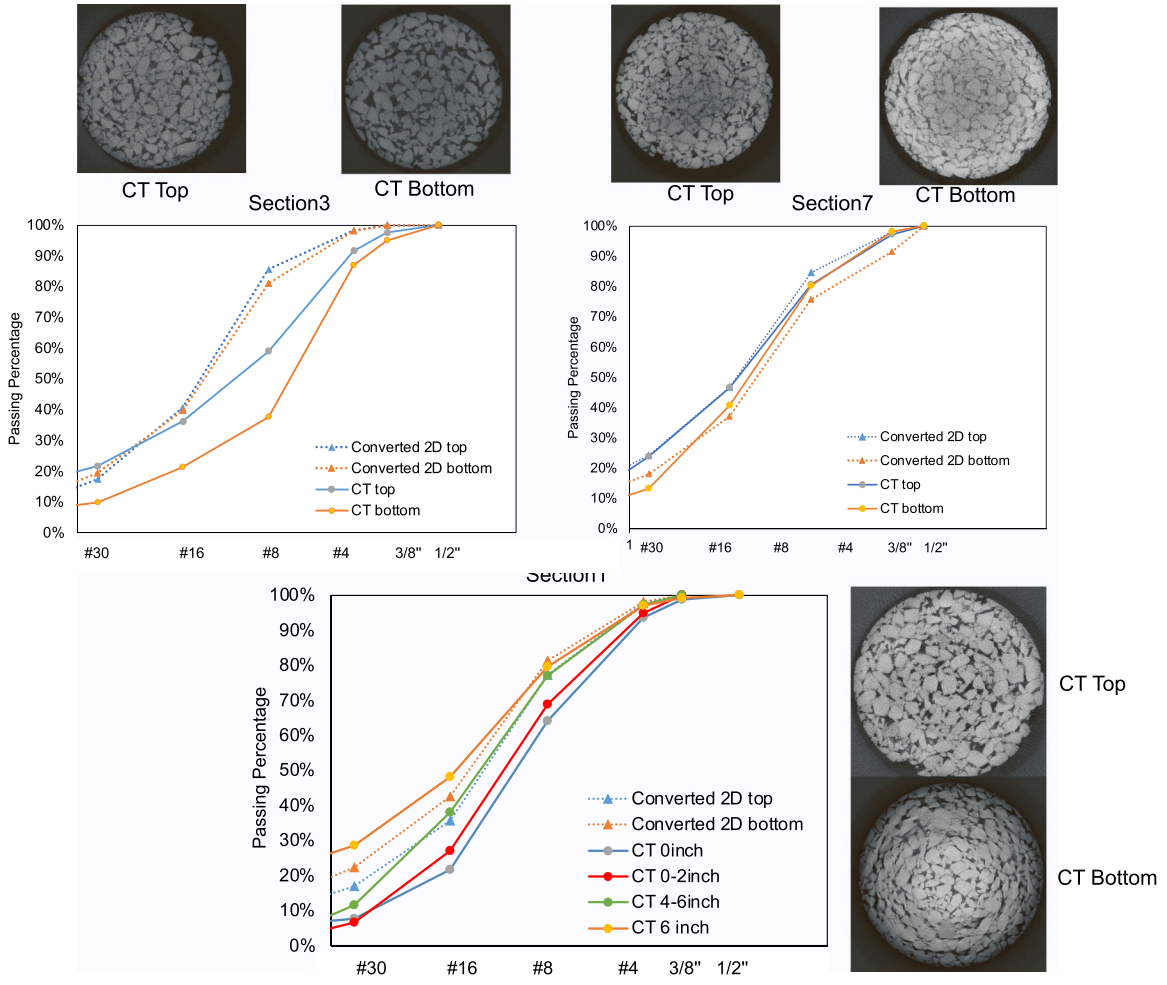


**Fig. 13.** CT-scan 2D gradation variation with layer depth for sections 1 (2020), 7 (2014), and 3 (2008).

pavement section but not the same sample. Furthermore, the 2D CT-scan derived gradations stem from one specific slice but the experimentally extracted gradation is an integrated gradation of a segment of the mixture in terms of thickness. Also, the differences for fines sized lower than *No*. 8 may be affected by the CT-scan resolution.

AV distribution with depth was summarized in Fig. 14 for three sections having a 6-year time gap among them. It was found that the porosity at the surface is higher than the inner porosity. This is also verified by studies of Masad et al. [43] and Ling et al. [44]. In terms of aging, there is a trend of higher AV for all sections in the middle and the bottom for the less-aged sections, this represents the clogging of the porous structure with time because of fines downward movement by washing and gravity. The exception to this trend was section 7 (2014), where the surface layer presented the highest AV content, explained by the clear raveling of the surface course of the PAM.

### 3.5. Mechanical analysis

Volumetric analysis showed that the cores evaluated by means of $E^*$ had AV of 14 % (section 1), 19 % (section 5), and 18 % (section 4). By comparing sections 1 and 5, it was possible to see that section 1 had a stiffer modulus both in terms of binder (Fig. 9), and in terms of mixture (also given the lower AV content), as shown in Fig. 15. Section 4 presented the lowest stiffness of all evaluated mixes (although information regarding binder is missing). It was believed that, although aging stiffens the binder, being subjected to cycles of moisture and freeze-thaw, together with the increased brittleness of the asphalt concrete, caused damage and a subsequent modulus reduction. On the other hand, in all cases, the $E^*$ test for the same mixes in a partially saturated condition (from 25 % to 31 % saturation) resulted both in increase in modulus and reduction in phase angle. This reflected a trend that the existence of capillary forces and the presence of moisture within the voids' structure can considerably change a parameter of utmost importance for pavement design, which is also potentially true for full-depth porous mixtures. The observed increase in mixture modulus with partial saturation can be rationalized through the findings of Rueda et al. [40], who suggest that the filling of voids with an incompressible fluid, such as water, leads to a relative increase in modulus. However, this phenomenon is more complex: water penetration and partial saturation pose risks in colder regions like Illinois, where temperatures often dip below 0°F ( − 20°C) during colder months. The expansion of water within voids during freezing induces microcracks and significantly weakens the bond between asphalt and aggregates. This observation is further supported by the increased susceptibility to disintegration observed for sections subjected to more freeze-thaw cycles. The cumulative effect of freeze-thaw cycles inevitably induces damage upon the PAM mixture layer, which is reflected in modulus testing results, despite the observed stiffening at the binder scale due to aging.

## 4. Conclusions

This research addressed different aspects of PAM performance in Chicago, and how performance evolved with time. PAM cores were obtained from seven different locations, each one having different years in service, constructed from 2008 to 2020. The analyses performed highlighted challenges that limit a more extensive use of PAMs in cold climates. The findings of this research were derived from non-destructive analyses of cores' texture and internal structure, as well as from multi-scale tests performed both to asphalt binders and mixtures. Notable conclusions include:

- Macrotexture (Sa and Sq) slightly increased with aging, attributed to aggregate raveling. Skewness (Ssk) also increased with aging, indicating the accumulation of fines between coarse particles on the pavement surface, leading to the obstruction of texture channel structures.
- An aging gradient within the PAM layer was observed, and it is not caused exclusively by thermal factors. The level of exposure to UV radiation emerges as another significant influence that should be considered.
- Ductility analysis using poker chip showed a significant level of deterioration of the asphalt binder with sections with more than 8 years in service, for both the top and the bottom of the PAM layer. Consequently, conventional rehabilitation methods such as milling and resurfacing of the top few inches of the asphalt layer are not feasible for full-depth PAM sections in Chicago.
- Control of binder content is crucial for PAM durability, because the interlocking of the mineral skeleton relies more heavily on the asphalt binder only. Lower-than-designed binder contents compromise durability, given that satisfactory bonding of particles protects against issues like raveling. Implementation of Balanced Mix Design (BMD) for PAMs must address this complexity to ensure long-term performance and durability.
- For "older" sections, binder content at the bottom of the layer was lower due to the "washing" effect that occurs with time. As water flows through the PAM layer, it has the potential to carry away aggregate particles coated with binder, as well as the binder itself detached from aggregates' surfaces.
- The increase in fine aggregate content and clogging of the surface layer was captured through gradation analysis of the material passing the #200 sieve in aged sections. The gradation analysis of aged sections also revealed a reduction in the quantity of coarse particles at the surface, particularly in the #3/8 fraction, indicating the effects of raveling.
- The distribution of air voids within PAM layers is not uniform. The middle of the layer consistently has the lowest AV (%). The AV gradient is more pronounced in sections that had been in service for more than 8 years. A higher concentration of voids was observed near the surface. While pore clogging remains a concern, other factors such as raveling may contribute to the increase in AV at the surface over time.
- Mixtures' $|E^*|$ was sensitive to binder stiffness for sections of the same age; however, as section age increases, the effect of other damage sources, such as moisture damage and freeze-thaw, are more relevant, leading to a decrease in $|E^*|$.

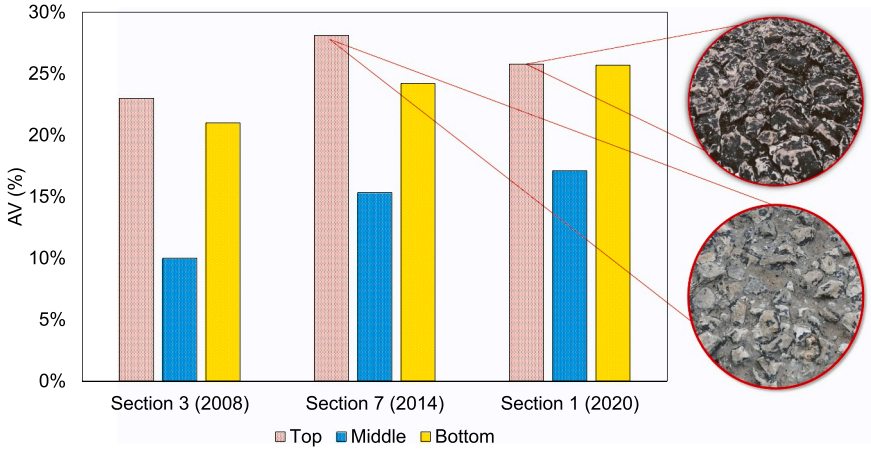


**Fig. 14.** Air voids distribution with thickness for sections 1, 3, and 7.

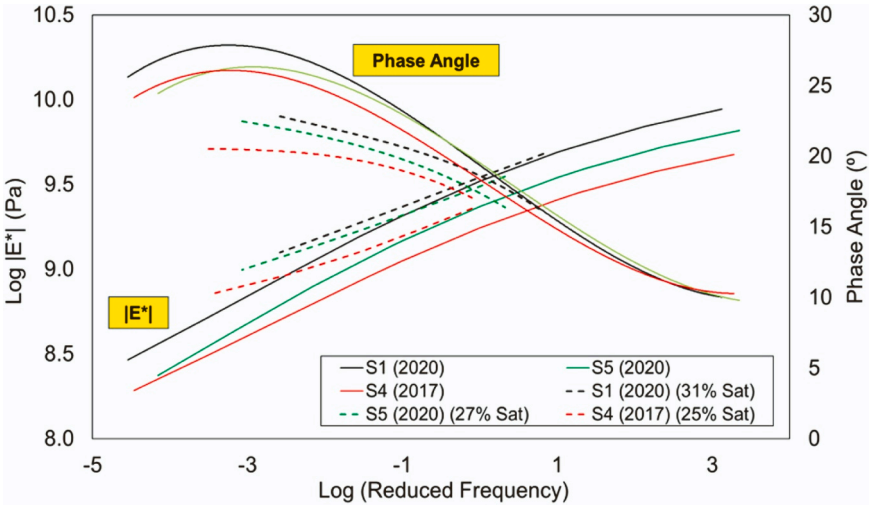


**Fig. 15.** |*E**| and Phase Angle for sections 1 (2020), 5 (2020), and 4 (2017) at different saturation levels.

- At certain degrees of saturation, increase in relative moisture content led to an increase in stiffness. However, efforts should be directed to improve resistance against moisture damage and freeze-thaw effects, given that the combination of saturation and loading will ultimately accelerate these damage mechanisms.

The findings of this research shed light on critical points that need to be considered to optimize the durability of PAMs in cold regions. Future research efforts should prioritize developing Balanced Mix Design methodologies that address these challenges, with a focus on controlling binder content and enhancing resistance to environmental factors prevalent in cold climates. The prioritization of the use of asphalt binders that can retain satisfactory ductility levels even after aging would slightly compensate for the more severe effects of moisture penetration and freeze-thaw effects happening within PAM layers. The construction of these asphalt layers also needs to be improved in order to avoid an AV (%) gradient that can potentially store water for more time than desired, contributing to moisture-induced damage and expansion during freezing effects. By addressing some of these issues, a more widespread and sustainable implementation of PAMs in cold regions can be achieved, contributing to the resilience of infrastructure systems in these areas.

## CRediT authorship contribution statement

**Renan Santos Maia:** Writing – review & editing, Writing – original draft, Project administration, Methodology, Investigation, Formal analysis. **Ramez Hajj:** Writing – review & editing, Resources, Project administration, Methodology, Funding acquisition, Formal analysis, Conceptualization. **Yujia Lu:** Writing – review & editing, Writing – original draft, Methodology, Investigation, Formal analysis.

## Declaration of Competing Interest

The authors declare that they have no known competing financial interests or personal relationships that could have appeared to influence the work reported in this paper.

## Data Availability

Data will be made available on request.

## Acknowledgements

The authors thank the Illinois-Indiana Sea Grant (Grant Number NA18OAR4170082) for funding this study. The authors also gratefully thank the Chicago Department of Transportation for assisting with identifying field sections, providing mix design information, and providing the cores, and STATE testing for their help in coring and transferring specimens to the research team. The authors also thank staff from the Institute for Genomic Biology at the University of Illinois for performing CT scans.

## References

[1] K. Song, S. You, J. Chon, Simulation modeling for a resilience improvement plan for natural disasters in a coastal area, Environ. Pollut. 242 (2018) 1970–1980.
[2] Y. Qiao, A.R. Dawson, T. Parry, G. Flintsch, W. Wang, Flexible pavements and climate change: A comprehensive review and implications, Sustainability 12 (2020) 1057.
[3] K.P. Kwiatkowski, I. Stipanovic Oslakovic, H. TerMaat, A. Hartmann, P. Chinowsky, G.P. Dewulf, Modeling cost impacts and adaptation of freeze–thaw climate change on a porous asphalt road network, J. Infrastruct. Syst. 26 (2020) 04020022.
[4] H. Zhu, M. Yu, J. Zhu, H. Lu, R. Cao, Simulation study on effect of permeable pavement on reducing flood risk of urban runoff, Int. J. Transp. Sci. Technol. 8 (2019) 373–382.
[5] M. Saleh, L. Hashemian, Addressing climate change resilience in pavements: major vulnerability issues and adaptation measures, Sustainability 14 (2022) 2410.
[6] X. Guan, J. Wang, F. Xiao, Sponge city strategy and application of pavement materials in sponge city, J. Clean. Prod. 303 (2021) 127022.
[7] M. Markus, D.J. Wuebbles, X.-Z. Liang, K. Hayhoe, D.A. Kristovich, Diagnostic analysis of future climate scenarios applied to urban flooding in the chicago metropolitan area, Clim. Change 111 (2012) 879–902.
[8] A. Kermanshah, S. Derrible, Robustness of road systems to extreme flooding: using elements of gis, travel demand, and network science, Nat. Hazards 86 (2017) 151–164.
[9] J.M.P. Mayora, R.J. Piña, An assessment of the skid resistance effect on traffic safety under wet-pavement conditions, Accid. Anal. Prev. 41 (2009) 881–886.
[10] R. Santos Maia, S. Lacerda Costa, F.J. Craveiro Cunto, V.T.F. Castelo Branco, Relating weather conditions, drivers' behavior, and tire-pavement friction to the analysis of microscopic simulated vehicular conflicts, J. Transp. Eng., Part B: Pavements 147 (2021) 04021037.
[11] K. Zhang, J. Kevern, Review of porous asphalt pavements in cold regions: the state of practice and case study repository in design, construction, and maintenance, J. Infrastruct. Preserv. Resil. 2 (2021) 1–17.
[12] M.A. Lebens, B. Troyer, Porous Asphalt Pavement Performance in Cold Regions - Report No MN/RC 2012-12, Technical Report, Minnesota Department of Transportation, Office of Materials and Road Research, 2012. Available on: ⟨https://hdl.handle.net/20.500.14153/mndot.2884⟩.
[13] P.T. Weiss, M. Kayhanian, J.S. Gulliver, L. Khazanovich, Permeable pavement in northern north american urban areas: research review and knowledge gaps, Int. J. Pavement Eng. 20 (2019) 143–162.
[14] P. Singhvi, J.J.G. Mainieri, H. Ozer, B.K. Sharma, I.L. Al-Qadi, K.L. Morse, Impacts of field and laboratory long-term aging on asphalt binders, Transp. Res. Rec. 2676 (2022) 336–353.
[15] R. Jing, A. Varveri, X. Liu, A. Scarpas, S. Erkens, Laboratory and field aging effect on bitumen chemistry and rheology in porous asphalt mixture, Transp. Res. Rec. 2673 (2019) 365–374.
[16] F. Frigio, E. Pasquini, M.N. Partl, F. Canestrari, Use of reclaimed asphalt in porous asphalt mixtures: laboratory and field evaluations, J. Mater. Civ. Eng. 27 (2015) 04014211.
[17] M.R. Thompson, B.J. Dempsey, Evaluation of freeze-thaw durability of stabilized materials, Transportation Research Record (1976).
[18] R.B. Kogbara, E.A. Masad, D. Woodward, P. Millar, Relating surface texture parameters from close range photogrammetry to grip-tester pavement friction measurements, Constr. Build. Mater. 166 (2018) 227–240.
[19] M. Medeiros Jr, L. Babadopulos, R. Maia, V. Castelo Branco, 3d pavement macrotexture parameters from close range photogrammetry, Int. J. Pavement Eng. (2021) 1–15.
[20] M.L. Williams, R.F. Landel, J.D. Ferry, The temperature dependence of relaxation mechanisms in amorphous polymers and other glass-forming liquids, J. Am. Chem. Soc. 77 (1955) 3701–3707.
[21] A. Filonzi, S. Komaragiri, R. Hajj, M. Trevino, D. Hazlett, E. Mahmoud, A. Bhasin, A method to evaluate the tensile strength and ductility of asphalt binders using a thin confined film, Int. J. Pavement Eng. (2022) 1–12.
[22] A. Bhasin, A. Filonzi, S. Komaragiri, R. Hajj, T. Seay, M. Trevino, Parts and Sample Preparation Guide for the Poker Chip or Asphalt Ductility Test 2021. Available on: https://dataverse.tdl.org/dataset.xhtml?persistentId=doi:10.18738/T8/KTCNVK, 10.18738/T8/KTCNVK.
[23] A. Vyas, Y. Wang, R. Hajj, E. Jahns, Investigation of factors affecting modified asphalt binder development and performance using the poker chip test, Constr. Build. Mater. 403 (2023) 133037.
[24] P. Marsac, N. Piérard, L. Porot, W. Van den Bergh, J. Grenfell, V. Mouillet, S. Pouget, J. Besamusca, F. Farcas, T. Gabet, et al., Potential and limits of ftir methods for reclaimed asphalt characterisation, Mater. Struct. 47 (2014) 1273–1286.
[25] B. Hofko, M.Z. Alavi, H. Grothe, D. Jones, J. Harvey, Repeatability and sensitivity of ftir atr spectral analysis methods for bituminous binders, Mater. Struct. 50 (2017) 1–15.
[26] H. Li, Z. Feng, A.T. Ahmed, M. Yombah, C. Cui, G. Zhao, P. Guo, Y. Sheng, Repurposing waste oils into cleaner aged asphalt pavement materials: a critical review, J. Clean. Prod. 334 (2022) 130230.
[27] Y. Lu, B. Asadi, R. Hajj, Rheological, mechanical, microscopic, and chemical characterization of asphalt binders at extended aging levels, J. Mater. Civ. Eng. 35 (2023) 04023256.
[28] E. Masad, V. Jandhyala, N. Dasgupta, N. Somadevan, N. Shashidhar, Characterization of air void distribution in asphalt mixes using x-ray computed tomography, J. Mater. Civ. Eng. 14 (2002) 122–129.
[29] L. Tashman, E. Masad, J. D'Angelo, J. Bukowski, T. Harman, X-ray tomography to characterize air void distribution in superpave gyratory compacted specimens, Int. J. Pavement Eng. 3 (2002) 19–28.
[30] J. Hu, Z. Qian, Y. Liu, Y. Xue, Microstructural characteristics of asphalt concrete with different gradations by x-ray ct, J. Wuhan. Univ. Technol. Mater. Sci. Ed. 32 (2017) 625–632.

[31] J. Liu, Y. Wang, S. Wang, Q. Liu, B. Yu, Q. Wang, Use of x-ray computed tomography to evaluate the gradual behaviour of air voids in asphalt mixtures during permanent deformation, Int. J. Pavement Eng. (2022) 1–19.
[32] A.H. Norhidayah, M.Z.H. Mahmud, P.J. Ramadhansyah, Air void characterisation in porous asphalt using x-ray computed tomography, Adv. Mater. Res.Trans. Tech. Publ. 911 (2014) 443–448.
[33] J.B. Król, R. Khan, A.C. Collop, The study of the effect of internal structure on permeability of porous asphalt, Road. Mater. Pavement Des. 19 (2018) 935–951.
[34] Y. Zhao, X. Wang, J. Jiang, L. Zhou, Characterization of interconnectivity, size distribution and uniformity of air voids in porous asphalt concrete using x-ray ct scanning images, Constr. Build. Mater. 213 (2019) 182–193.
[35] A. Filonzi, R. Hajj, A.d.F. Smit, A. Bhasin, Validation of inverse stereology generation of two dimensional area gradations for computational modelling of asphalt mixtures, Road. Mater. Pavement Des. 22 (2021) 2197–2211.
[36] S.D. Wicksell, The corpuscle problem: a mathematical study of a biometric problem, Biometrika (1925) 84–99.
[37] P. Zhang, Microstructure Generation of Asphalt Concrete and Lattice Modeling of Its Cracking Behavior under Low Temperature (Ph.D. thesis), North Carolina State University, 2004.
[38] J. Schindelin, I. Arganda-Carreras, E. Frise, V. Kaynig, M. Longair, T. Pietzsch, S. Preibisch, C. Rueden, S. Saalfeld, B. Schmid, et al., Fiji: an open-source platform for biological-image analysis, Nat. Methods 9 (2012) 676–682.
[39] A.J. Enríquez-León, T.D. de Souza, F.T.S. Aragão, D. Braz, A.M.B. Pereira, L.P. Nogueira, Determination of the air void content of asphalt concrete mixtures using artificial intelligence techniques to segment micro-ct images, Int. J. Pavement Eng. 23 (2022) 3973–3982.
[40] E.J. Rueda, S. Caro, B. Caicedo, Influence of wetting-drying cycles on the linear viscoelastic properties of asphalt mixtures, Constr. Build. Mater. 393 (2023) 132072.
[41] M.W. Witzcak, Simple performance test for superpave mix design, volume 465, Transp. Res. Board (2002).
[42] B. Hofko, L. Porot, A. Falchetto Cannone, L. Poulikakos, L. Huber, X. Lu, K. Mollenhauer, H. Grothe, Ftir spectral analysis of bituminous binders: reproducibility and impact of ageing temperature, Mater. Struct. 51 (2018) 1–16.
[43] E. Masad, B. Muhunthan, N. Shashidhar, T. Harman, Quantifying laboratory compaction effects on the internal structure of asphalt concrete, Transp. Res. Rec. 1999 (1681) 179–185.
[44] S. Ling, Y. Sun, D. Sun, D. Jelagin, Pore characteristics and permeability simulation of porous asphalt mixture in pouring semi-flexible pavement, Constr. Build. Mater. 330 (2022) 127253.